ARTICLES

Photothermal Correlation Spectroscopy of Gold Nanoparticles in Solution†

Pedro M. R. Paulo,‡,§ Alexander Gaiduk,‡ Florian Kulzer,‖,⊥ S. F. Gabby Krens,‖ Herman P. Spaink,‖ Thomas Schmidt,‡ and Michel Orrit*,‡

Institute of Physics, Leiden University, P.O. Box 9504, 2300 RA Leiden, The Netherlands, and Institute of Biology, Leiden University, P.O. Box 9505, 2300 RA Leiden, The Netherlands

Received: August 1, 2008; Revised Manuscript Received: September 16, 2008

We demonstrate correlation analysis of the photothermal signal from gold nanoparticles diffusing in solution. Our experimental setup is primarily optimized for large detection volumes and therefore has a relatively low numerical aperture (0.25). This requirement limits light collection and detection efficiency, but we can nevertheless detect particles as small as 20 nm in diameter in 100 μs. Photothermal correlation spectroscopy (PCS) in water and in water:glycerol mixtures gives access to characteristic diffusion times of some tens of milliseconds. Diffusion is enhanced for high pump intensities, due to the increased temperature around the particle. The photothermal signal at the detector arises from the interference of the scattered probe beam and a reference field. In the forward configuration, the reference is the transmitted probe beam itself. In the backward configuration, the reference wave is a reflection by a nearby interface. It has an optical phase difference depending on the distance of the particle to the reflecting interface. The backward signal also includes the directly modulated scattering signal. Potential applications of photothermal correlation in biological labeling are demonstrated on bacteriophage virus particles carrying 20 nm gold labels.

Introduction

The unique properties of gold and silver nanoparticles make them attractive objects for fundamental and applied research,[1–16] as probes in nanophotonics,[17–19] and biological labeling and sensing.[20–30] Compared to organic dyes and semiconductor nanocrystals, gold nanoparticles are free from photoinduced bleaching or blinking, facilitating continuous observation of the same particle over long times. The absorption spectrum of a nanoparticle depends on its size, shape, and local environment,[12–16] a property exploited in multicolor labeling schemes,[15,21] but the low photoluminescence quantum yield makes detection of single particles difficult. Dark-field scattering by single metal particles is difficult for diameters less than 40 nm, because their scattering cross-section scales with squared volume.[12] As interferometric signals scale as the scattered field instead of the scattered intensity, they provide access to smaller sizes.[31] This approach was recently implemented for photothermal detection of single metal nanoparticles in two different ways: photothermal interference contrast[22,32,33] (PIC) and photothermal heterodyne imaging[34–37] (PHI). In photothermal detection, a nanoparticle is illuminated with a pump beam, usually at a wavelength close to the particle's surface plasmon resonance. The absorbed energy is dissipated as heat to the surrounding environment. The detected signal arises from scattering of a second beam, the probe, by the local thermally induced variation of refraction index. The variation in scattered intensity is proportional to the particle's absorption cross-section, which scales with the volume, and allows for observation of smaller objects. For instance, using PHI with high numerical aperture optics (NA = 1.4), Berciaud et al. detected individual gold particles with diameters down to 1.4 nm (only 67 gold atoms) with a signal-to-noise ratio SNR > 10, an integration time of 10 ms and a temperature rise on the particle surface of only about 2 K.[34] This was achieved on an immobilized sample, and the same method was used for single-particle tracking in biological samples,[27] providing two-dimensional trajectories of membrane receptors labeled with 5 nm-gold in live cells at video rates.

For diffusion faster than video rate, one can employ correlation analysis of the fluctuations of the photothermal signal, in analogy to the widely known technique of fluorescence correlation spectroscopy.[38–41] In fluctuation spectroscopy, the observation volume is reduced to dimensions small enough that the diffusion-induced statistical number fluctuations of molecules (or particles) lead to measureable signal fluctuations. The large absorption cross-sections of gold nanoparticles (3–4 orders of magnitude higher than that of common fluorescent labels[31]) make them appealing for fluctuation spectroscopy. The strength of the photothermal signal and the absence of saturation at high pump powers (unless heating damage occurs) compensates for the absence of photoluminescence.

Hereafter, we present a general discussion of photothermal correlation spectroscopy (PCS), and compare results in two experimental configurations we used to analyze the free diffusion of gold nanoparticles in solution.

---

† Part of the "Hiroshi Masuhara Festschrift".
* Corresponding author. Fax: +31 71 520 5910. E-mail: orrit@molphys.leidenuniv.nl.
‡ Leiden Institute of Physics.
§ Present address: Centro de Química Estrutural - Complexo 1, Instituto Superior Técnico, Av. Rovisco Pais, 1049-001 Lisboa, Portugal.
‖ Leiden Institute of Biology.
⊥ Present address: ICFO - Institut de Ciencies Fotoniques, Mediterranean Technology Park, 08860 Castelldefels (Barcelona), Spain.

11452   *J. Phys. Chem. C, Vol. 113, No. 27, 2009*

Paulo et al.
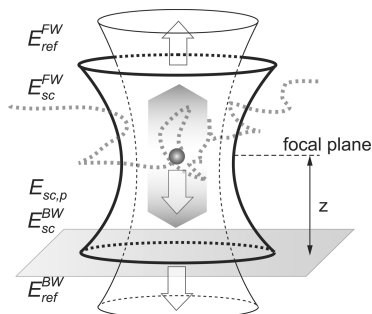
Figure 1. Scheme of a photothermal correlation experiment in solution, with nanoparticles diffusing in the common focus of two laser beams. Thin line: heating (pump) beam; thick line: probe beam. In the backward mode, the photothermal signal arises from interference of $\vec{E}_{sc}^{BW}$ (modulated part of the scattered field), and $\vec{E}_{sc,p}$ (static part of the back-scattered field by the particle itself) with $\vec{E}_{ref}^{BW}$ (field reflected by the bottom interface of the measurement cell). In the forward mode, $\vec{E}_{sc}^{FW}$ interferes with $\vec{E}_{ref}^{FW}$, the transmitted probe field. The dashed gray line represents the diffusion trajectory of a particle through the detection volume.

Methods

We analyze correlations of the interferometric photothermal signal (PHI),[34] obtained when an intensity-modulated heating beam induces a time-varying change of temperature (ΔT) and thus of refractive index (Δn) around the nanoparticle. Scattering of a nonresonant probe beam off the time-dependent refractive index profile ($\Delta T \times \partial n/\partial T$) produces a scattered field ($\vec{E}_{sc}(t)$) with a component varying at the modulation frequency (Ω). Interference of the scattered field with a reference field ($\vec{E}_{ref}$, often referred to as the "local oscillator") produces a signal at the modulation frequency, which is retrieved by a lock-in amplifier (heterodyne detection). Two detection configurations are possible:

(i) In the backward mode (BW), the signal is collected in the back-scattered geometry by the same illumination objective. The reference field $\vec{E}_{ref}^{BW}$ is provided by a reflection of the probe beam at an optical interface close to the detected object. This configuration is convenient because it requires only one objective, but it has a disadvantage. Because of the optical phase difference between the scatterer and the surface, the photothermal signal changes sign over a time corresponding to diffusion over a half-wavelength. The correlation signal is strong only for short times (see below for a more detailed discussion).

(ii) In the forward mode (FW), the reference field $\vec{E}_{ref}^{FW}$ is the transmitted probe beam itself (Figure 1). This configuration requires a second objective for light collection but it provides a very good detectivity.

In both experimental configurations, the detector measures the total intensity ($I_{det} \propto |\vec{E}_{ref} + \vec{E}_{sc}|^2$) resulting from the interference of the reference and scattered fields, and the lock-in selects the component of the signal varying at the modulation frequency Ω. We assume these two fields to be in the same spatial mode. The photothermal signal (S_{PHD}) mainly arises from the time-dependent part of the interference term, $2Re[E_{ref}^* E_{sc}(t)]$, but the scattered intensity $|\vec{E}_{sc}|^2$ also includes a modulated component. We briefly outline the derivation of the analytical equation for S_{PHD} for a nanoabsorber heated in the focus of the probe beam, considering the interference term only, and following the treatment given in ref 37.

The modulated signal power (S_{PHD}) is proportional to the scattered field $|\vec{E}_{sc}(t)| \approx 1/4\pi\varepsilon_0\omega_0\lambda^2|\vec{p}|$, radiated by an equivalent dipole $|\vec{p}| \approx 2n\Delta n \cdot V \cdot |\vec{E}_{probe}|$ resulting from the change of the dielectric permittivity $\Delta(n^2)$ in the probed volume V. The permittivity change

is modulated at frequency Ω and is proportional to the power absorbed by the particle ($P_{abs} = \sigma_{abs}P_{heat}/A$)

$$S_{PHD} \approx \frac{1}{\pi\omega_0}n\frac{\partial n}{\partial T}\frac{P_{abs}P_{probe}}{\lambda^2 C_p\Omega} \qquad (1)$$

where σ_{abs} is the absorption cross-section of the particle, P_{heat} is the average heating power, A and ω_0 are the effective area of the beam cross section and the focal radius (or beam waist), C_p is the heat capacity per unit volume of the solution (water: 4.18×10^6 J K^{-1} m^{-3}), and λ is the wavelength of the scattered light (probe).

For an ideal detector, the noise of the photothermal detection arises only from the photon noise in the detected probe beam. The signal-to-noise ratio (SNR$_{PHD}$) for the shot-noise-limited photothermal detection is given by

$$SNR_{PHD} \approx \frac{1}{\pi\omega_0}n\frac{\partial n}{\partial T}\frac{P_{abs}}{\lambda^2 C_p\Omega}\sqrt{\frac{P_{probe}\Delta t}{h\nu}} \qquad (2)$$

where $h\nu$ is the energy of the probe photon and Δt is the integration time. As follows from eq 2, if the probe light is not absorbed, SNR$_{PHD}$ can be indefinitely increased by increasing P_{probe}. That opens a possibility to detect very small particles with the photothermal signal.

The signal-to-noise ratio should be roughly equivalent for the backward and forward configurations in the case of shot noise limited detection, except at low modulation frequencies, for which forward scattering is more efficient.[37,42]

An important issue for biological compatibility of the PHD is the increase of the temperature around a nanoabsorber. The temperature at the surface of a particle is given by[37,43]

$$\Delta T_{surf} = \frac{P_{abs}}{4\pi\kappa R} \qquad (3)$$

where κ is the thermal conductivity of the medium (0.6 W K^{-1} m^{-1} for water) and R is the particle's radius. The temperature elevation around the particle decreases to half its value at the surface at a distance of one particle radius. In the above estimate, only heating by the pump is considered; the probe contribution is neglected. Assuming equal powers for probe (633 nm) and pump (514 nm), the fraction of the temperature rise due to the probe is about 4% for particles less than 60 nm in diameter and about 13% for 80 nm. In our experiments, the power of the probe light is at least 1 order of magnitude smaller than the power of the heating light. Thus the influence of the probe light on the temperature rise is less than 1%.

The relationship of the surface temperature increase ΔT_{surf} with the integration time of the photothermal signal for particles of different diameters with a fixed SNR is shown in Figure 2. The same SNR can be achieved either with a longer integration time and a lower temperature rise or a shorter integration and higher temperature. Since the SNR is proportional to NA^2 for the constant probe power (see Supporting Information A), one has to increase either the temperature rise or the integration time for a lower NA (see Figure 2), if one wishes to recover a comparable SNR.

In our PCS experiments, the heating and probe beams are focused into overlapping volumes of the colloidal solution (colloid) in which the nanoparticles diffuse. We consider separately two possible experimental configurations.

(i) Forward Mode. Because the two interfering fields propagate in the same direction, the phase mismatch between the reference and the scattered fields is weak. Residual phase mismatches can arise from spatial mode mismatch (including the Gouy phase

Gold Nanoparticles in Solution

J. Phys. Chem. C, Vol. 113, No. 27, 2009 **11453**
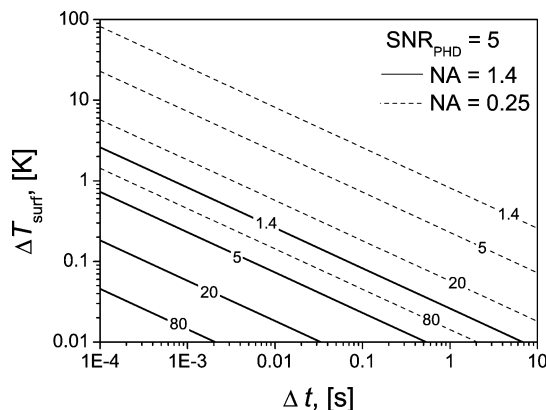
Figure 2. The dependence of the temperature rise upon the integration time Δt at a fixed SNR_{PHD} (=5) for gold particles of given diameters (1.4, 5, 20, and 80 nm) and NA = 1.4 (solid lines) and NA = 0.25 (dashed lines). The values used for calculations are ω_0 = 250 nm (for NA=1.4), Ω = 500 kHz, P_{probe} = 10 mW, λ_{probe} = 633 nm. Residual heating from probe absorption has been neglected.
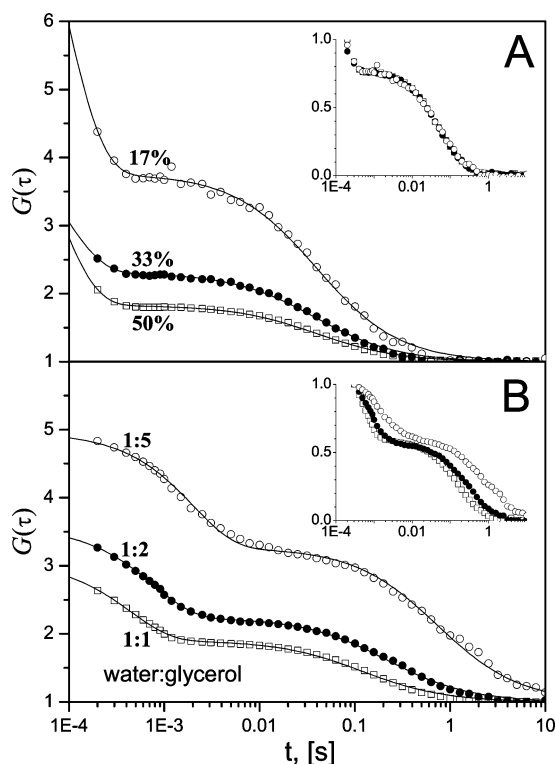
Figure 3. Photothermal autocorrelation obtained for gold particles with 80 nm diameter diluted in pure water (A) and in water:glycerol mixtures (B) in the backward mode. The labels indicate the percentage of stock sample solution in case (A) and the water:glycerol composition in case (B). The solid lines are fits with eq 6 (see parameters in the text). The insets show the same experimental data normalized to the initial value to facilitate comparison of the characteristic times.

shift[44]), or from lateral shifts of the particle with respect to the optical axis. Therefore, the photothermal signal only rarely changes sign and has a nonzero average value. The autocorrelation function (ACF) of the time traces of the photothermal signal $S_{PHD}(t)$ can be normalized in the usual way and provides information about the diffusion dynamics of the particles across the focus

$$G(\tau) = \frac{\langle S_{PHD}(t) S_{PHD}(t+\tau) \rangle}{\langle S_{PHD} \rangle^2} \qquad (4)$$

We fitted the experimental ACFs with the usual FCS expression for a two-dimensional Brownian diffusion,

$$G(\tau) = 1 + \frac{1}{N}(1 + \tau/\tau_d)^{-1} \qquad (5)$$

where N is the average number of particles in the detection volume and τ_d is the diffusion time of the particle across the detection volume. The approximation of 2-D diffusion is valid in our setup because of the reduced numerical aperture. The axial extent of the detection volume is much larger than its diameter.[45] However, as discussed below, the conventional expressions of Brownian diffusion to PCS only apply at low enough heating power, because heating around the particle may change the local viscosity and the diffusion rate. This change was evaluated through numerical simulations of a model with a position-dependent diffusion coefficient, which will be reported elsewhere.

(ii) Backward Mode. In the backward mode, the photothermal signal arising from interference with the reflection has a random phase, and averages out in the diffusion perpendicular to the interface. In the correlation function, this signal contributes a fast component corresponding to diffusion within a half-wavelength, but does not contribute to the slow component corresponding to diffusion across the much larger focal volume. An additional signal arises from time-modulated scattering by the particle (i.e., the difference in scattering strength between hot and cold particle-environment system). This signal can be seen as the interference of the modulated part of the scattered field, $\vec{E}_{sc}^{BW}(t)$, with the static part of the scattered field, $\vec{E}_{sc,p}$. Being obviously free from any phase mismatch, this signal has a fixed sign, provides an average photothermal signal, and contributes a slow component when the particle diffuses in the focal volume.

Accordingly, the backward (BW) photothermal signal can be expressed as the sum of two terms, $S_{PHD}^{BW} = 2Re[E_{sc,p}^* E_{sc}^{BW}(t)] + 2Re[E_{ref}^{BW*} E_{sc}^{BW}(t)]$. The distance between the diffusing particle and the optical interface introduces a phase mismatch between the scattered $\vec{E}_{sc}^{BW}(t)$ and the reflected $\vec{E}_{ref}^{BW}$ fields, causing the second term in S_{PHD}^{BW} to change sign upon diffusion along the optical axis (see Figure 1). Therefore, for large enough particles, or for an out-of-focus reflection, the photothermal signal arises mainly from the first term of S_{PHD}^{BW}, and the photothermal bursts then present a dominant sign. The correlation function of the total photothermal signal contains two contributions, one from the first term corresponding to diffusive motion across the beam and a second, fast component from the second term in S_{PHD}^{BW} corresponding to diffusion across the interference fringes (the cross-term averages out). This situation is completely analogous to that of FCS on a mirror,[48] with a different "effective fringe visibility" $V = r/a$, given by the relative contributions r and a of the reflected $\vec{E}_{ref}^{BW}$ and scattered $\vec{E}_{sc,p}$ fields (note that this effective visibility strongly depends on particle size and reflection intensity).

As in FCS on a mirror, two fluctuation processes take place on different time-scales: the diffusion through the whole observation volume (slow fluctuations, fixed sign) and diffusion between the optical fringes of different brightness (fast fluctuations, random sign). We fitted the ACFs for backward mode detection with the model developed for FCS on a mirror (eq 6)[46−48]

$$G(\tau) = 1 + \frac{1}{N}[1 + n_f \exp(-\tau/\tau_f)](1 + \tau/\tau_d)^{-1} \qquad (6)$$

where N is the average number of particles in the detection volume, n_f is a constant related to the fringe visibility, τ_f is a characteristic time for diffusion between the fringes, and τ_d is the diffusion time across the transverse direction of the detection volume. The last term in eq 6 can be recognized as the term for 2-D Brownian diffusion (see eq 5).

11454 *J. Phys. Chem. C, Vol. 113, No. 27, 2009*

Paulo et al.

Experimental Section

The experimental setup is a modification of the home-built photothermal microscope reported previously.[45] Briefly, the heating beam is provided by the 514.5 nm line of an argon ion laser (Coherent Inc., Innova 310). The intensity of the heating beam is modulated by an acousto-optic modulator (AA Opto-Electronic, modulator AA.MT110/A1.5-VIS and RF driver AA.MOD.110.D47), which is driven by a square wave at the modulation frequency $\Omega = 500$ kHz. The probe beam is provided by a Helium−Neon laser (Melles Griot, 25LHP991−230, $\lambda = 632.8$ nm). Both beams are expanded by telescopes, combined by a dichroic mirror (AHF/Chroma F43−525) and guided to the sample through a microscope objective (UPLSAPO10x, numerical aperture NA = 0.4, and working distance 3.1 mm). The heating laser and probe laser were focused into spots with a radius ω_0 of 1.2−1.4 μm and a Rayleigh length of about 15 μm. The axial overlap of two foci is controlled by knife-edge profile scanning.[49] The effective NA for the underfilled objective lens is calculated to be $NA_{eff} = 0.25$. The detection volume is estimated to be 200 fl, which is larger, by more than 2 orders of magnitude, than the volumes typically used in FCS. This extended detection volume is advantageous for applications in high-throughput screening, as discussed previously.[45] Slight variations in the detection volume of the backward configuration compared to the forward configuration are due to differences in the numerical aperture of the collection objectives.

In the backward mode (BW), the same objective is used for collection. The collected light passes through a cleanup interference filter (Semrock, MaxLine 632.8 nm) to block reflections from the heating beam. The filtered beam is focused onto an analog avalanche photodiode (APD; New Focus, 1801FS-AC-M). In forward mode (FW), a second objective (Mitutoyo MPlanApo20x, numerical aperture 0.28, working distance 30 mm) is used for collection. The light collected is cleaned from the heating laser by a dichroic mirror (AHF/Chroma F43−525) and an interference filter (Semrock, MaxLine 632.8 nm). Another avalanche photodiode detector (Femto, HCA-S-200M-SI) is used for the forward detection. The APD output is fed into a lock-in amplifier (Stanford Research Systems, SR844) tuned to the modulation frequency. The lock-in amplifier detects the signal with a time constant of 20−40 μs. The time traces of the photothermal signal were acquired for up to 400 s with a time-bin of 0.1 ms.

Samples of gold colloids with diameters of 20 and 80 nm (British Biocell International, EM.GC20 and EM.GC80) were prepared by dissolving an adequate volume of stock solution in ultrapure water or glycerol. The concentrations of the stock solutions of gold colloids are 7×10^{11} and 1.1×10^{10} particle/mL for 20 and 80 nm particle sizes respectively (according to the supplier's specifications; the diluted suspensions of gold colloids are identified by the volume ratio x:y of dilution). The measurements were performed in cells made from two glass coverslips and a rubber O-ring which was attached to the bottom coverslip. Prior to cell assembly, all parts were carefully cleaned to avoid colloid aggregation. The glass coverslips were sonicated in isopropanol (absolute grade) for 10 min, dried, and treated in a UV-ozone cleaner for another 10 min. Samples of bacteriophage virus with 20 nm gold colloids attached were prepared by genetically engineering M13 phages to display the biotin epitope on the coating proteins P3 (3−5 copies/phage) and P8 (2700 copies/phage).[50] The engineered phages were then mixed with an excess quantity of gold colloids coated with streptavidin (British Biocell International, ArraySTP20). The concentration of viable phages was determined by titrations and

the values obtained are in the order of 5.4×10^7 to 4.4×10^8 cfu/mL. For the photothermal measurements, the phage stock solutions were diluted to about 1:10 (v/v) in PBS buffer (pH 7.4).

Results and Discussion

We begin this section with results of photothermal correlation spectroscopy measured in backward mode for gold particles of 80 nm in diameter, diffusing freely in water. For convenience reasons, most measurements were done in this configuration, although the signal-to-noise ratio was much better in the forward mode. For 80 nm particles, the signal bursts are strong enough to be clearly discriminated against the noise. The effect of dilution, illustrated in Figure 3A, is an increase in contrast of the autocorrelation function. The shape of the autocorrelation curves is not affected by dilution (inset in Figure 3A), which confirms that particle−particle interaction or aggregation are negligible. Figure 3B shows the effect of dilution by glycerol, with a shift of the autocorrelation curves to longer times (inset) as the viscosity increases. The slower diffusion in the water-glycerol mixture reveals a short component at about 100 microseconds, which we attribute to diffusion through the interference pattern (see the Methods section).

We hereafter discuss fits of eq 6 to the correlation curves of Figure 3. Figure 4 shows that the average numbers of particles in the detection volume obtained from the fits (N_{fit}) are in good agreement with bulk values (N_{estim}), confirming that the bursts arise from individual particles. For the water:glycerol mixtures, it is possible to retrieve both diffusion times τ_f and τ_d (in pure water, τ_f falls below our time resolution). According to the model for FCS on a mirror,[46] the ratio of the diffusion times τ_f and τ_d should not depend on the viscosity of the medium, but only on the beam waist ω_0, the probe wavelength λ and the refraction index of the medium n

$$\frac{\tau_d}{\tau_f} = 4\pi^2 n \frac{\omega_0{}^2}{\lambda^2} \quad (7)$$

Indeed, we verified that the values of τ_d/τ_f are independent of the mixture composition and agree within experimental uncertainty with the value of 286 predicted with eq 7 (refractive index of glycerol $n_g = 1.47$, $\omega_0 = 1.4$ μm). The values calculated for the ratio of the diffusion times τ_d and τ_f fitted from the curves in Figure 3B are 320 ± 37, 306 ± 25, and 316 ± 65 for 1:1, 1:2, and 1:5 compositions of water:glycerol mixtures, respectively. This supports our interpretation of the fast signal fluctuations as diffusion in an interference pattern. The values fitted for the pre-exponential factor n_f in eq 6 decrease with the fraction of glycerol in the mixture: 1.3, 1.1, and 0.75 for compositions 1:1, 1:2, and 1:5, respectively. As the fraction of glycerol increases, the index of refraction of the mixture should approach that of the bottom glass interface ($n_{glass} = 1.5$) and the reflected fraction of the probe beam decreases, thus leading to a decrease of the fringe visibility and n_f (see the Methods section).

Increasing the heating intensity raises the particle's temperature as well as that of its surroundings, which leads to a faster diffusion. This was verified experimentally by increasing the power of the heating laser and following the decrease in the diffusion times fitted from the respective autocorrelation curves (Figure 5). The decrease in the diffusion time τ_d for the suspensions in pure water is not as pronounced as that for the water:glycerol mixtures. The behavior of the diffusion times is well described by the fits in Figure 5, which assume heating-

Gold Nanoparticles in Solution

J. Phys. Chem. C, Vol. 113, No. 27, 2009 **11455**
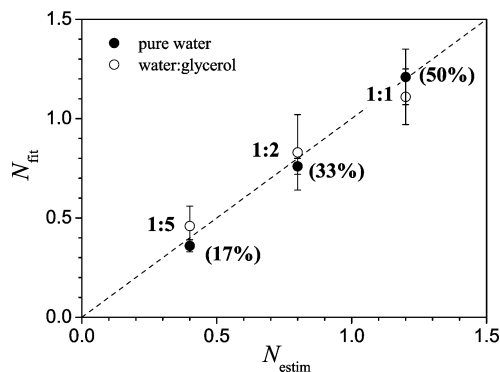
Figure 4. Values of the average number of particles (N_{fit}) in the detection volume estimated from the data in Figure 3 fitted with eq 6 versus estimated concentrations of particles in suspension, N_{estim}. The uncertainty bars represent the empirical standard deviation for repeated experiments; each data point corresponds to at least three separate correlation measurements. The labels indicate the dilution factors: volume percentage of particle sample for water, and the composition of water:glycerol for the mixtures. As expected, the particle concentration depends only on the dilution, not on the viscosity. The dashed line represents $N_{fit} = N_{estim}$.
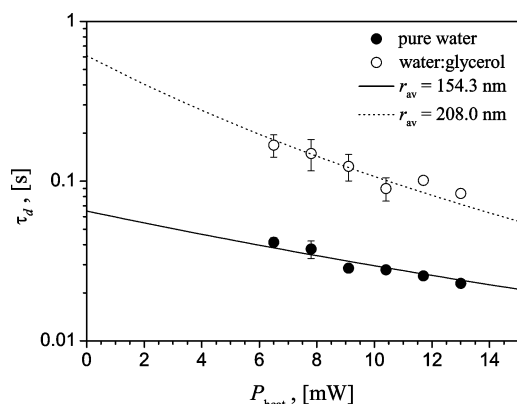

Figure 5. Diffusion time of 80 nm-diameter gold particles in pure water (full circles) and in a water:glycerol mixture (open circles) as a function of the power of the heating laser, P_{heat}, measured in the backward mode. The error bars represent the standard deviation for at least three consecutive measurements of the same sample. The curves are obtained in a model where the diffusion time scales with a local viscosity averaged over a sphere with adjustable radius r_{av} (see Supporting Information B). The best fits for the water (solid line) and water:glycerol mixture (dashed line) give the averaging radii of $r_{av} = 154.3$ and 208.0 nm, respectively.

induced changes of the liquid's properties, in particular the viscosity η (see Supporting Information B), around each nanoparticle. The model predicts a decrease of the diffusion time by a factor of up to 7.2 (2.8) for water:glycerol (pure water) in the considered range of heating powers. In water:glycerol mixtures, a more accurate analysis should consider the local change of mixture composition via the Soret effect,[51,52] neglected here.

In the forward mode, as no interference effect occurs, no short component appears in the correlation (Figure 6). The photothermal signal is much stronger. We could easily detect 20 nm diameter gold particles diffusing in water (highly diluted to obtain the concentration of about one single particle in the detection volume). The diffusion time, 15.7 ms, compares well with the estimated diffusion time of 15.4 ms for a single particle with 20 nm in diameter (results of the observation are not shown), according to the Stokes−Einstein relation for the diffusion coefficient D (see Supporting Information B). The
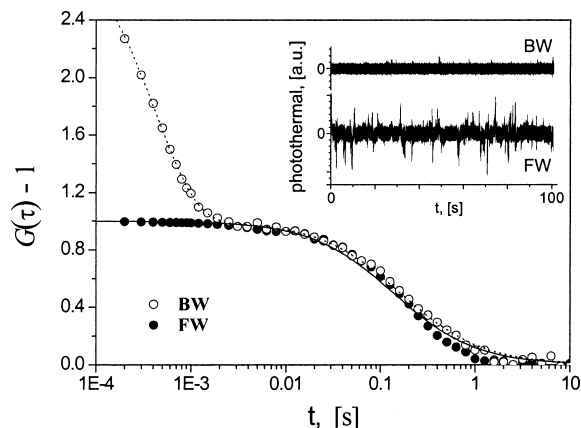
Figure 6. Comparison of photothermal correlation in the backward mode (BW, open circles) and in the forward mode (FW, full circles) for gold particles with 80 nm diameter in a 1:1 water:glycerol mixture. The short component of the backward mode is not observed in the forward mode. Lines indicate fits of the data with eq 6 (for BW) and with eq 5 (for FW) with the diffusion time $\tau_d^{BW} = 181 \pm 27$ ms and $\tau_d^{FW} = 164 \pm 27$ ms, respectively. The insert shows examples of photothermal traces. Although it is not clear at the insert resolution, the sign of the bursts in the FW trace is dominantly negative.
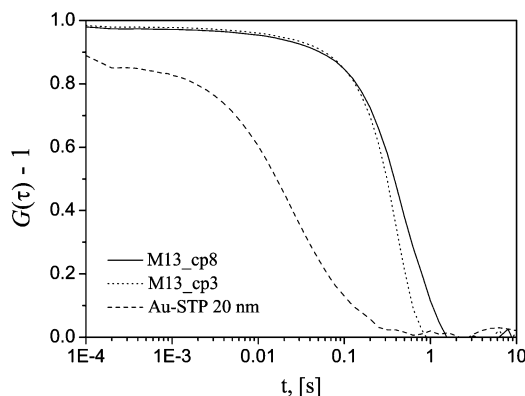
Figure 7. Autocorrelation curves obtained for M13 bacteriophage viruses labeled with 20 nm gold particles at the coating proteins P8 (M13_cP8, full line) and at coating proteins P3 (M13_cP3, dotted line) in the forward mode. The dashed line is the autocorrelation curve obtained for free labels, streptavidin-coated gold particles with 20 nm diameter (Au-STP 20 nm) in aqueous environment (control measurement). The ACF curves are normalized for visual comparison of the characteristic diffusion times.

values predicted for the diffusion time of dimers (25.0 ms) and aggregates up to hexamers (28.4 ms) are significantly longer.[53]

The heating effect of the photothermal measurement on the medium properties was taken into account. The maximum temperature rise at the surface of a particle at the objective focus, estimated from eq 3 with a heating beam power of 52 mW ($I_{heat} = 1.2$ MW/cm^2, with $\omega_0 = 1.2$ μm), was found to be $\Delta T_{surf} = 51$ K. This temperature increase may appear too high for certain applications, but one should not forget that the present detection time is short (100 μs), that each particle stays only a fraction of a second in the focus, and that the temperature rise decreases to 25 K already 20 nm away from the particle surface.

Our results show that forward-scattering is clearly more appropriate for high-throughput detection in solution. However, the interference effect, which occurs in the backward mode, could be useful to study diffusion in confined geometries, like micro- and nanochannels, where interactions with the channel walls could interfere with diffusion dynamics or diffusion processes perpendicular to the main flow of the fluid. The fringe

patterning of the detection volume enables addressing diffusion processes on length scales of a half-wavelength. Such a concept was demonstrated in studies of protein diffusion in tubular structures within cells using the technique of FCS on a mirror.[46]

Finally, we present PCS measurements in forward mode for bacteriophage viruses labeled with 20 nm gold particles. The photothermal bursts of these objects are much longer than those of the free gold particles. A M13 bacteriophage is a rod-like shaped virus with a length of approximately 800 nm and a width of 8 nm. As a consequence, the autocorrelation curves reveal longer diffusion times for the phages than for the free strepta-vidin-coated 20 nm gold particles (by approximately 1 order of magnitude, see Figure 7). The diffusion time obtained for the streptavidin-coated 20 nm gold particles is 21.3 ± 0.8 ms, slightly longer than that of noncoated particles (15.7 ms), but significantly shorter than the estimated time for clusters.[53] The correlation shape for gold-labeled phages clearly differs from that of the free particles, which suggests that the diffusion dynamics of these large objects is more complex. This may be related to their high aspect ratio and to the local heterogeneity of the temperature profile around the virus, as its length is comparable to the transverse dimensions of the detection volume. Currently, we are using the phages expressing biotin to the coat proteins P8 (cP8), that form the cylindrical body of the phages, and the coat proteins P3 (cP3), that are in the phages' extremities, to attach the streptavidin-coated gold particles. Some limited phage aggregation may take place because of possible multiple labeling.

Another issue that deserves closer attention is the effect of heating on the viability of the phages. The heating powers used for detection of these samples correspond to a surface temperature rise of up to 51 K for 20 nm gold labels. However, this temperature decreases as the inverse distance from the particle's center. Furthermore, the residence times of the detected objects in the observation volume range from some tens to hundreds of milliseconds, which might be sufficiently short to avoid substantial heating damage for many biological species showing no aggregation.[54] Heating damage can always be minimized by sacrificing detection bandwidth or by reducing the heating power, and compensating the lower signal with an increase in the probe power.

Conclusions

We have presented the combination of photothermal microscopy and correlation spectroscopy. This method was applied to characterize the diffusion of gold nanoparticles in liquid solution. Two principal modes of operation were considered, backward and forward detection. In the backward mode, we observed axial striation of the detection volume by interference between the back-scattered light and the interface reflection; this effect gives rise to an additional short-time component in the diffusional correlation function and can be understood quantitatively by a model developed earlier to describe FCS on a mirror. We verified experimentally that increasing the heating power leads to shorter diffusion times, as it is expected from the larger temperature change around the particle.

In the forward mode, the interference effect is eliminated and the signal intensity increases. This allowed us to detect gold particles as small as 20 nm in diameter and to perform photothermal correlation spectroscopy with a time-resolution of 100 microseconds. The size limit of 20 nm could be improved with high-numerical aperture optics, however our experimental setup was designed for a compromise between the detection efficiency and the size of the observation volume.[45] An extended

detection volume is advantageous for applications in high-throughput screening because it enhances the capacity of processing "large" sample volumes. Being free from bleaching and blinking, gold nanoparticles are attractive labels for screening applications with single-object sensitivity. This screening method opens the way to multistage sorting steps, and to the rejection of false negatives to arbitrarily low levels. Finally, we show how photothermal correlation can be applied to detect gold-labeled bacteriophage viruses and study their diffusion.

Supporting Information Available: (A) Calculations of the photothermal signal-to-noise ratio and numerical aperture. (B) Diffusion in water and water:glycerol mixtures and influence of the heating. This material is available free of charge via the Internet at http://pubs.acs.org.

References and Notes

(1) Burda, C.; Chen, X.; Narayanan, R.; El-Sayed, M. A. Chemistry and Properties of Nanocrystals of Different Shapes. *Chem. Rev.* **2005**, *105*, 1025–1102.

(2) Rosi, N. L.; Mirkin, C. A. Nanostructures in Biodiagnostics. *Chem. Rev.* **2005**, *105*, 1547–1562.

(3) Lu, H. P. Site-specific Raman spectroscopy and chemical dynamics of nanoscale interstitial systems. *J. Phys.: Condens. Matter.* **2005**, *17*, R333–R355.

(4) Luo, X.; Morrin, A.; Killard, A. J.; Smyth, M. R. Application of Nanoparticles in Electrochemical Sensors and Biosensors. *Electroanalysis* **2006**, *18*, 319–326.

(5) Drake, C.; Deshpande, S.; Bera, D.; Seal, S. Metallic nanostructured materials based sensors. *Int. Mater. Rev.* **2007**, *52*, 289–317.

(6) Raimondi, F.; Scherer, G. G.; Kötz, R.; Wokaun, A. Nanoparticles in Energy Technology: Examples from Electrochemistry and Catalysis. *Angew. Chem., Int. Ed.* **2005**, *44*, 2190–2209.

(7) Aiken, J. D.; Finke, R. G. A review of modern transition-metal nanoclusters: their synthesis, characterization, and applications in catalysis. *J. Mol. Catal. A. Chem.* **1999**, *145*, 1–44.

(8) Astruc, D.; Lu, F.; Aranzaes, J. R. Nanoparticles as Recyclable Catalysts: The Frontier between Homogeneous and Heterogeneous Catalysis. *Angew. Chem., Int. Ed.* **2005**, *44*, 7852–7872.

(9) Narayanan, R.; El-Sayed, M. A. Catalysis with Transition Metal Nanoparticles in Colloidal Solution: Nanoparticle Shape Dependence and Stability. *J. Phys. Chem. B* **2005**, *109*, 12663–12676.

(10) Panigrahi, S.; Basu, S.; Praharaj, S.; Pande, S.; Jana, S.; Pal, A.; Ghosh, S. K.; Pal, T. Synthesis and Size-Selective Catalysis by Supported Gold Nanoparticles: Study on Heterogeneous and Homogeneous Catalytic Process. *J. Phys. Chem. C* **2007**, *111*, 4596–4605.

(11) Ghosh, S. K.; Pal, T. Interparticle Coupling Effect on the Surface Plasmon Resonance of Gold Nanoparticles: From Theory to Applications. *Chem. Rev.* **2007**, *107*, 4797–4862.

(12) Kreibig, U.; Vollmer, M. *Optical Properties of Metal Clusters*; Springer Series in Materials Science; Springer: Berlin, 1995; Vol. 25.

(13) Link, S.; El-Sayed, M. A. Shape and size dependence of radiative, non-radiative and photothermal properties of gold nanocrystals. *Int. Rev. Phys. Chem.* **2000**, *19*, 409–453.

(14) Link, S.; El-Sayed, M. A. Optical Properties and Ultrafast Dynamics of Metallic Nanocrystals. *Annu. Rev. Phys. Chem.* **2003**, *54*, 331–366.

(15) Kelly, K. L.; Coronado, E.; Zhao, L. L.; Schatz, G. C. The Optical Properties of Metal Nanoparticles: The Influence of Size, Shape, and Dielectric Environment. *J. Phys. Chem. B* **2003**, *107*, 668–677.

(16) Jain, P. K.; Huang, X.; El-Sayed, I. H.; El-Sayed, M. A. Review of some interesting surface plasmon resonance-enhanced properties of noble metal nanoparticles and their applications to biosystems. *Plasmonics* **2007**, *2*, 107–118.

(17) Salerno, M.; Krenn, J. R.; Lamprecht, B.; Schider, G.; Ditlbacher, H.; Felidj, N.; Leitner, A.; Aussenegg, F. R. Plasmon polaritons in metal

Gold Nanoparticles in Solution

J. Phys. Chem. C, Vol. 113, No. 27, 2009 **11457**

nanostructures: the optoelectronic route to nanotechnology. *Opto-Electron. Rev.* **2002**, *10*, 217–224.

(18) Ditlbacher, H.; Krenn, J. R.; Schider, G.; Leitner, A.; Aussenegg, F. R. Two-dimensional optics with surface plasmon polaritons. *Appl. Phys. Lett.* **2002**, *81*, 1762–1764.

(19) Khlebtsov, B.; Zharov, V.; Melnikov, A.; Tuchin, V.; Khlebtsov, N. Optical amplification of photothermal therapy with gold nanoparticles and nanoclusters. *Nanotechnology* **2006**, *17*, 5167–5179.

(20) Taton, T. A.; Mirkin, C. A.; Letsinger, R. L. Scanometric DNA Array Detection with Nanoparticle Probes. *Science* **2000**, *289*, 1757–1760.

(21) Schultz, S.; Smith, D. R.; Mock, J. J.; Schultz, D. A. Single-target molecule detection with nonbleaching multicolor optical immunolabels. *Proc. Nat. Acad. Sci.* **2000**, *97*, 996–1001.

(22) Cognet, L.; Tardin, C.; Boyer, D.; Choquet, D.; Tamarat, P.; Lounis, B. Single metallic nanoparticle imaging for protein detection in cells. *Proc. Nat. Acad. Sci.* **2003**, *100*, 11350–11355.

(23) Fritzsche, W.; Taton, T. A. Metal nanoparticles as labels for heterogeneous, chip-based DNA detection. *Nanotechnology* **2003**, *14*, R63–R73.

(24) Penn, S. G.; Hey, L.; Natanz, M. J. Nanoparticles for bioanalysis. *Curr. Opin. Chem. Biol.* **2003**, *7*, 609–615.

(25) Raschke, G.; Kowarik, S.; Franzl, T.; Sönnichsen, C.; Klar, T. A.; Feldmann, J.; Nichtl, A.; Kürzinger, K. Biomolecular Recognition Based on Single Gold Nanoparticle Light Scattering. *Nano Lett.* **2003**, *3*, 935–938.

(26) Blab, G. A.; Cognet, L.; Berciaud, S.; Alexandre, I.; Husar, D.; Remacle, J.; Lounis, B. Optical Readout of Gold Nanoparticle-Based DNA Microarrays without Silver Enhancement. *Biophys. J.* **2006**, *90*, L13–L15.

(27) Lasne, D.; Blab, G. A.; Berciaud, S.; Heine, M.; Groc, L.; Choquet, D.; Cognet, L.; Lounis, B. Single Nanoparticle Photothermal Tracking (SNaPT) of 5-nm Gold Beads in Live Cells. *Biophys. J.* **2006**, *91*, 4598–4604.

(28) Lakowicz, J. R. Plasmonics in biology and plasmon-controlled fluorescence. *Plasmonics* **2006**, *1*, 5–33.

(29) Moller, R.; Fritzsche, W. Metal nanoparticle-based detection for DNA analysis. *Curr. Pharm. Biotechnol.* **2007**, *8*, 274–285.

(30) Huang, X. H.; Jain, P. K.; El-Sayed, I. H.; El-Sayed, M. A. Gold nanoparticles: interesting optical properties and recent applications in cancer diagnostic and therapy. *Nanomedicine* **2007**, *2*, 681–693.

(31) van Dijk, M. A.; Tchebotareva, A. L.; Orrit, M.; Lippitz, M.; Berciaud, S.; Lasne, D.; Cognet, L.; Lounis, B. Absorption and scattering microscopy of single metal nanoparticles. *Phys. Chem. Chem. Phys.* **2006**, *8*, 3486–3495.

(32) Boyer, D.; Tamarat, P.; Maali, A.; Lounis, B.; Orrit, M. Photothermal Imaging of Nanometer-Sized Metal Particles Among Scatterers. *Science* **2002**, *297*, 1160–1163.

(33) Boyer, D.; Tamarat, P.; Maali, A.; Orrit, M.; Lounis, B. Imaging single metal nanoparticles in scattering media by photothermal interference contrast. *Physica E* **2003**, *17*, 537–540.

(34) Berciaud, S.; Cognet, L.; Blab, G. A.; Lounis, B. Photothermal Heterodyne Imaging of Individual Nonfluorescent Nanoclusters and Nanocrystals. *Phys. Rev. Lett.* **2004**, *93*, 257402.

(35) Berciaud, S.; Cognet, L.; Tamarat, P.; Lounis, B. Observation of Intrinsic Size Effects in the Optical Response of Individual Gold Nanoparticles. *Nano Lett.* **2005**, *5*, 515–518.

(36) Berciaud, S.; Cognet, L.; Lounis, B. Photothermal Absorption Spectroscopy of Individual Semiconductor Nanocrystals. *Nano Lett.* **2005**, *5*, 2160–2163.

(37) Berciaud, S.; Lasne, D.; Blab, G. A.; Cognet, L.; Lounis, B. Photothermal heterodyne imaging of individual metallic nanoparticles: Theory versus experiment. *Phys. Rev. B* **2006**, *73*, 045424.

(38) Magde, D.; Elson, E.; Webb, W. W. Thermodynamic Fluctuations in a Reacting Systems - Measurement by Fluorescence Correlation Spectroscopy. *Phys. Rev. Lett.* **1972**, *29*, 705–708.

(39) Koppel, D. E.; Axelrod, D.; Schlessinger, J.; Elson, E. L.; Webb, W. W. Dynamics of Fluorescence Marker Concentration as a Probe of Mobility. *Biophys. J.* **1976**, *16*, 1315–1329.

(40) Aragón, S. R.; Pecora, R. Fluorescence Correlation Spectroscopy as a Probe of Molecular Dynamics. *J. Chem. Phys.* **1976**, *64*, 1791–1803.

(41) *Single Molecule Detection in Solution*; Zander, Ch., Enderlein, J., Keller, R. A., Eds.; Wiley-VCH Verlag Berlin GmbH: Berlin, 2002; Chapter 2.

(42) The criterion defined in ref. [37] for the low frequency regime is $\Omega \ll \Omega_C$, with $\Omega_C = 2D \, (2\pi n/\lambda)^2$. Using this expression we estimate $\Omega_C \approx 8$ MHz; our experiments were performed at a modulation frequency $\Omega = 500$ kHz, so we expect a better signal-to-noise ratio in the forward configuration relative to the backward configuration.

(43) Pitsillides, C. M.; Joe, E. K.; Wei, X.; Anderson, R. R.; Lin, C. P. Selective cell targeting with light-absorbing microparticles and nanoparticles. *Biophys. J.* **2003**, *84*, 4023–4032.

(44) Hwang, J.; Moerner, W. E. Interferometry of a single nanoparticle using the Gouy phase of a focused laser beam. *Opt. Commun.* **2007**, *280*, 487–491.

(45) Kulzer, F.; Laurens, N.; Besser, J.; Schmidt, T.; Orrit, M.; Spaink, H. P. Photothermal Detection of Individual Gold Nanoparticles: Perspectives for High-Throughput Screening. *ChemPhysChem.* **2008**, *9*, 1761–1766.

(46) Etienne, E.; Lenne, P.-F.; Sturgis, J. N.; Rigneault, H. Confined diffusion in tubular structures analyzed by fluorescence correlation spectroscopy on a mirror. *Appl. Opt.* **2006**, *45*, 4497–4507.

(47) Lenne, P.-F.; Etienne, E.; Rigneault, H. Subwavelength patterns and high detection efficiency in fluorescence correlation spectroscopy using photonic structures. *Appl. Phys. Lett.* **2002**, *80*, 4106–4108.

(48) Rigneault, H.; Lenne, P.-F. Fluorescence correlation spectroscopy on a mirror. *J. Opt. Soc. Am. B* **2003**, *20*, 2203–2214.

(49) Firester, A. H.; Heller, M. E.; Sheng, P. Knife-edge scanning measurements of subwavelength focused light beams. *Appl. Opt.* **1976**, *16*, 1971–1974.

(50) Kehoe, J. W.; Kay, B. K. Filamentous phage display in the new millennium. *Chem. Rev.* **2005**, *105*, 4056–4072.

(51) Duhr, S.; Braun, D. Why molecules move along a temperature gradient. *Proc. Natl. Acad. Sci. U.S.A.* **2006**, *103*, 19678–19682.

(52) Kempers, L. J. T. M. A comprehensive thermodynamic theory of the Soret effect in a multicomponent gas, liquid, or solid. *J. Chem. Phys.* **2001**, *115*, 6330–6341.

(53) The variation of the estimated diffusion time for the clusters is not monotonic with the cluster size due to the interplay between two counteracting effects: the increase in the hydrodynamic radius of the cluster, which makes diffusion slower and the higher absorbed power that increases the temperature rise around the object and, thus, accelerates diffusion. Note that a further complication, coupling between the plasmon resonances of the aggregated particles, was neglected in these estimates.

(54) Stehr, J.; Hrelescu, C.; Sperling, R. A.; Raschke, G.; Wunderlich, M.; Nichtl, A.; Kürzinger, K.; Parak, W. J.; Klar, T. A.; Feldmann, J. Gold NanoStoves for Microsecond DNA Melting Analysis. *Nano Lett.* **2008**, *8*, 619–623.